Investigation of the performance of different wavelet-based fusions of SAR and optical images using Sentinel-1 and Sentinel-2 datasets

Hüseyin Duysak *1 ID **, Enes Yigit** 2 ID

1Karamanoglu Mehmetbey University, Engineering Faculty, Electrical Electronics Engineering, Karaman, Turkey
2Bursa Uludag University, Engineering Faculty, Electrical Electronics Engineering, Bursa, Turkey

ABSTRACT

In this study, the fusion of optical and synthetic aperture radar images with wavelet transform was investigated. Images are obtained from Sentinel-1 and sentinel-2 satellites. Images were decomposed by wavelet transform. The four main coefficients were obtained for different wavelet packages and up to ten decomposition levels. The coefficients were combined taking the maximum, minimum or mean. 1710 Fused images were obtained for all possible combinations in terms of different wavelet packets, decomposition levels and fusion rules. Fused images were evaluated according to the structural similarity index (SSI). It was seen that the missing regions in the optical images were improved in the fused images with the appropriate wavelet packets and highest SSI.

1. INTRODUCTION

Image fusion is the unification of different images. The fused image includes information from all images. Image fusion has a wide range of applications such as sensor networks, remote sensing and medical (James and Dasarathy, 2014; Khaleghi et al. 2013). On the other hand, multimodal image fusion is performed by using images of different sensors. Thus, more meaningful information than a single sensor can be obtained in the fused image. In remote sensing applications, the fusion of synthetic aperture radar (SAR) image and the optical image has become popular due to the specific properties of images. SAR is one of the most important imaging systems, since radar are independent of weather and environmental conditions such as dust, smoke and cloud. Therefore, SAR images are an important information source in the evaluation of hazardous situations such as earthquake, landslide and volcanic eruption. Technically, SAR systems electromagnetically illuminate earth surface and collects reflected signals from earth objects. The energy of the reflected signal depends on the moisture, shape, dielectric coefficient of the surface and sensor parameters such as frequency, polarization,

observation angle. On the other hand, optical imaging system (OIS) is based on passive sensor and passive imaging systems need external source such as solar. Optical image (OI) is obtained by collecting a reflected solar energy from earth objects. Thus, OI depends on spectral resolution (infrared, visible or ultraviolet) and weather conditions. In terms of spectral characteristic, OI are categorized as panchromatic (PAN), multispectral (MS) and hyperspectral images (HS). PAN images are obtained using sensors with a frequency range covering from visible to a portion near-infrared of the spectrum. MS sensors provide MS images having different bands of spectrum. Thus, MS images are higher spectral resolution than PAN, but lower spatial resolution. The HS sensor generates the image by collecting signal from more bands of spectrum than MS. Therefore, hyperspectral images have more spectral information than MS and PAN, but their spatial resolutions are lower than MS and PAN images (Kulkarni and Rege 2020).

Optical-Optical and Optical-SAR image fusion types have each specific beneficial for practical applications. Optical-optical image fusion can be used to increase spectral resolution. Optical-SAR fusion can be used for better evaluation of surface features of the study area like

identifying Antarctic Ice features (Shah et al. 2019), plant species detection (Rajah et al. 2018).

SAR and optical systems are mounted on plane or satellite (Kulkarni and Rege 2020). Today, there are many satellites that actively provide SAR and optical images for academic research. One of them is sentinel. While the radar-based Sentinel-1 satellite captures SAR images, Sentinel-2 satellite is based on optical imaging and captures multispectral images. Images of Sentinel satellites are used in various applications such as agriculture (Veloso et al. 2017) and evaluation of natural disasters (Ghorbanzadeh et al. 2020).

For a valuable evaluation, it is important to combine as much data as possible from both image sources in the fusion process. In this way, missing data in SAR or optical images caused by some situations such as weather conditions, system noise, or smoke can be effectively completed. One of the basis of level fusion technique is pixel-level fusion (PLF). PLF is more appropriate in remote sensing applications due to less information loss than decision and feature level fusion techniques. However, PLF needs high computational process. In PLF, the fused image is obtained by combining pixel values of different images. Thus, before the fusion, some pre-processing techniques such as registration, denoising may be required, especially in multimodal medical image fusion (Aslan et al. 2019).

Image fusion can be performed by different methods such as Intensity Hue Saturation (IHS), Principal Component analysis (PCA), multiresolution techniques, sparse representations. One of the most popular method of multiresolution techniques is the wavelet transform (Kulkarni and Rege 2020). In this study, the SAR and optical images are fused using wavelet transform. Images were analysed by wavelet transform and fused according to maximum, minimum and mean methods based a fusion rule. This fusion rule is one of the traditional methods used in wavelet based fusion (Hemdan, 2021; Pajares and Manuel de la Cruz 2004). Fused images were obtained using different wavelet packages and decomposition levels. The similarity between fused image and original images is determined by using quality metrics with peak signal to noise ratio (PSNR), mean square error (MSE), structural similarity index (SSI), entropy (H) and feature similarity index (FSI).

The remainder of this work is organized as follows; in the second part includes the wavelet-based fusion, dataset and quality metrics. The results of the images given in the third part; the conclusions are summarized in the last part.

2. METHOD

2.1. Wavelet Transform Based Image Fusion

Wavelet transform is one of the most popular multiresolution analyse techniques in signal/ image processing applications such as noise removal and compression. Wavelet transform decomposes the image into low and high frequency components using wavelet packages. Four main coefficients are obtained as lower resolution approximation (LL), vertical (LH), horizontal (HL), and diagonal (HH) (Hemdan, 2021; Pajares and Manuel de la Cruz 2004). These coefficients of different images can be used to constitute a new coefficient by means of a fusion rule. Therefore, the fusion of images can be obtained with the new coefficient.

2.2. Fusion Rule

The different images are decomposed by applying the discrete wavelet transform (DWT). The combination of coefficients (LL, LH, HL, HH) is merged according to a fusion rule.

The one of the basic rules is to obtain new coefficients by taking the maximum, minimum or mean value of the coefficients, and then the fused image is obtained by taking inverse discrete wavelet transform (IDWT) (Pajares and Manuel de la Cruz 2004). The fusion rule is summarized in Fig. 1.

Figure 1. Fusion Rule Block Diagram

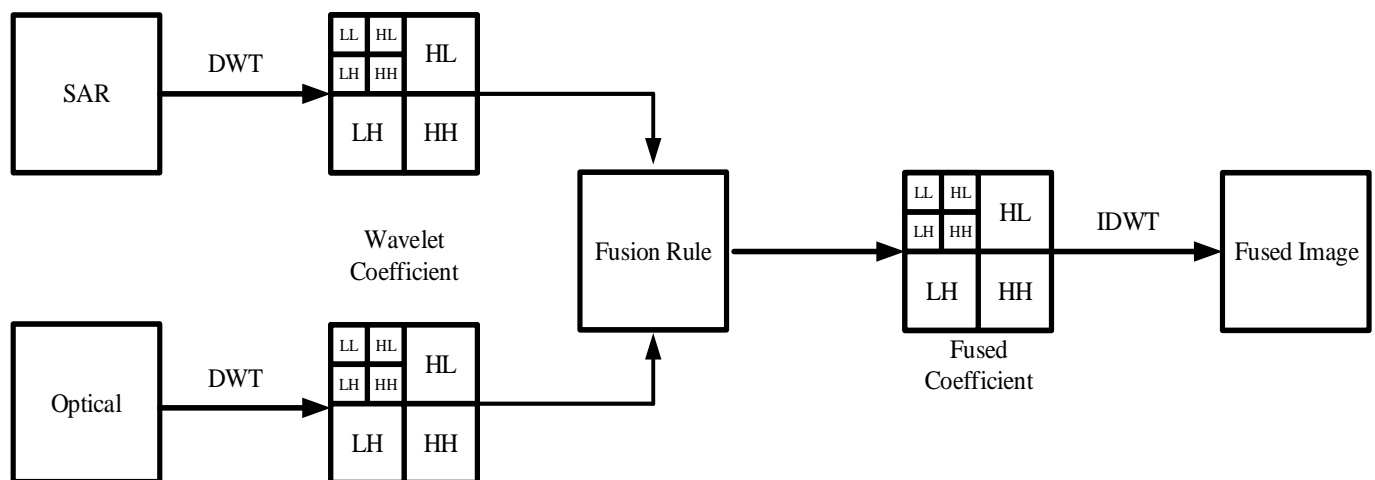### 2.3. Quality Metrics

PSNR, SSI, H, FSI and MSE were used to evaluate the performance of the fused images. H with a higher value indicates that the images contain more information. The PSNR value indicates the dominance of the input image in the fused image. If the SSI and FSI are high, this indicates that there is much similarity between the source image and the fused image. Besides, as MSE

decreases, the similarity between the input and the fused images increases (Kulkarni and Rege 2020).

2.4. Dataset

In this study, optical and SAR images captured by Sentinel-1 and Sentinel-2 satellites were used. The location of the site in the images, which is a part of the city of Karaman, is indicated in the Table 1.

Table 1. Geo-coordinates of site

Latitude Bound		Longitudes Bound	
North	37.235	West	33.177
South	37.197	East	33.277

Three datasets were downloaded from Copernicus Open Access Hub. Information of datasets are given in Table 2. The images were obtained by processing the datasets in sentinel application platform (SNAP) software (Foumelis et al. 2018). The optical images were obtained by applying the procedure given in Fig. 2. Prior to the subset the data were resampled to generate the image with the same spatial resolution since Sentinel-2 bands have different spatial resolution of 10, 20 and 60

meters. In order to constitute the SAR image, procedure shown in Fig. 3 were applied in SNAP. After the subset, calibration was applied to create the SAR image with accurate backscattering data. Then, Lee filter (Yommy et al. 2015) was performed to remove speckle noise. In order to represent pixels of images with correct locations, range doppler terrain correction was used. Finally, colorization of SAR image were obtained using vertical-vertical (VV) and vertical-horizontal (VH) polarization data. Red(R), green(G) and blue(B) components of coloured SAR image are obtained as follows,

$$R = Amplitude\ of\ VV\ backscattering\ data\ in\ dB$$
$$G = Amplitude\ of\ VH\ backscattering\ data\ in\ dB$$
$$B = \frac{Amplitude\ of\ VH\ backscattering\ data\ in\ dB}{Amplitude\ of\ VV\ backscattering\ data\ in\ dB}$$

Two optical (OP-1 and OP-2) and SAR (SAR1) images are given in Fig. 4. Optical images have some missing regions arising from various factors like smoke, dust or fog. These regions are shown with red rectangles.

Table 2. Information of Datasets

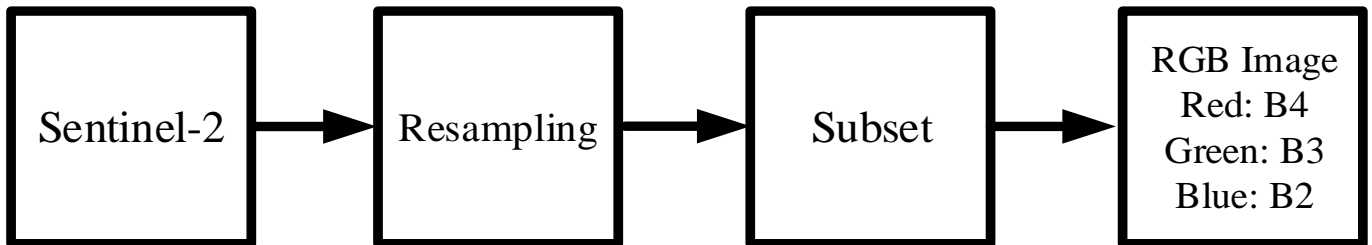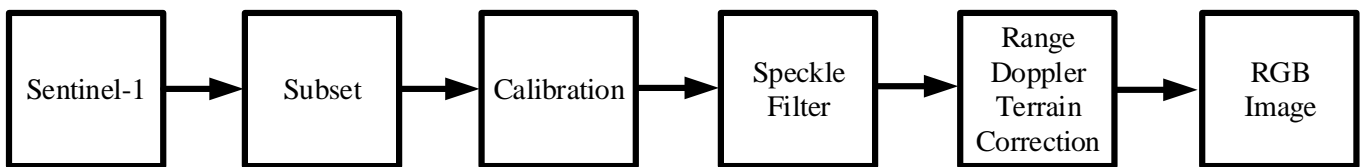| Image Label	Satellite	Acquisition Date	Acquisition Modes	Polarization	Level
OP1	Sentinel-2	08.01.2021	-	-	L1C
OP2	Sentinel-2	01.01.2021	-	-	L2A
SAR1	Sentinel-1	25.01.2021	*Interferometric Wide* (IW)	VV, VH	L1

Figure 2. Sentinel-2 Data Processing

Figure 3. Sentinel-1 Data Processing

3. RESULTS

The Optical and SAR images in Fig. 4 were analysed by applying wavelet transform with different wavelet packages including Daubechies (db1, db2, db3), Coiflets (coif1, coif2, coif3), Symlets (sym1, sym2, sym3), Fejer-Korovkin filters (fk4, fk6, fk8), Discrete Meyer (dmey), Biorthogonal (bior1.1, bior1.3, bior1.5) and Reverse Biorthogonal (rbior1.1, rbior1.3, rbior1.5) (Pajares and Manuel de la Cruz 2004). Wavelet coefficients of OP1, OP2 and SAR1 images are shown for "db1" wavelet package with level 1 in Fig. 5.

The optical images were fused with each other and the SAR image. Besides, images were analysed for decomposition level from 1 to 10. The combination of coefficients was performed by applying nine fusion rules in Table 3.

A total of 1710 fused images with 9 fusion rules, 19 wavelet packets and 10 decomposition levels can be obtained for each fusion application. In this study, 1710 fused images were obtained for each fusion of OP1-OP2, OP1-SAR1 and OP2-SAR1 images. Fused images were evaluated using quality metrics. Missing regions in optical images were evaluated in terms of clearness.

(a)

(b)
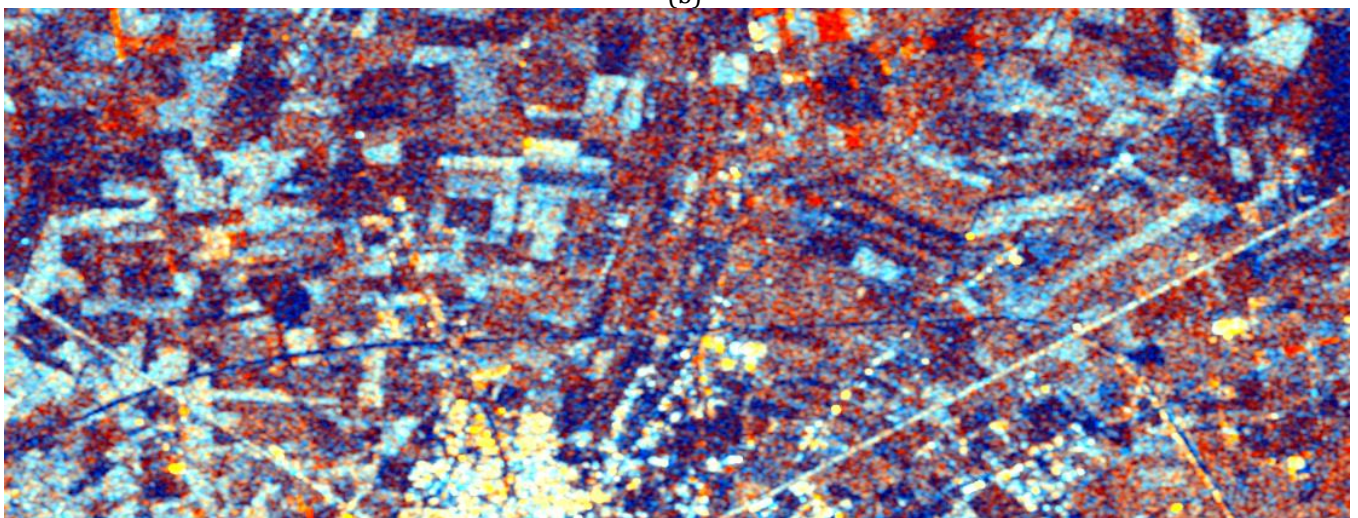
(c)

Figure 4. Sentinel 1 and Sentinel 2 dataset (a) OP1: Optical image from Sentinel-2 on 08 January 2021, (b) OP2: Optical image from Sentinel-2 on 01 January 2021 (c) SAR1: SAR RGB Image from Sentinel-1 IW- L1 ground range detected (GRD) on 25 January 2021
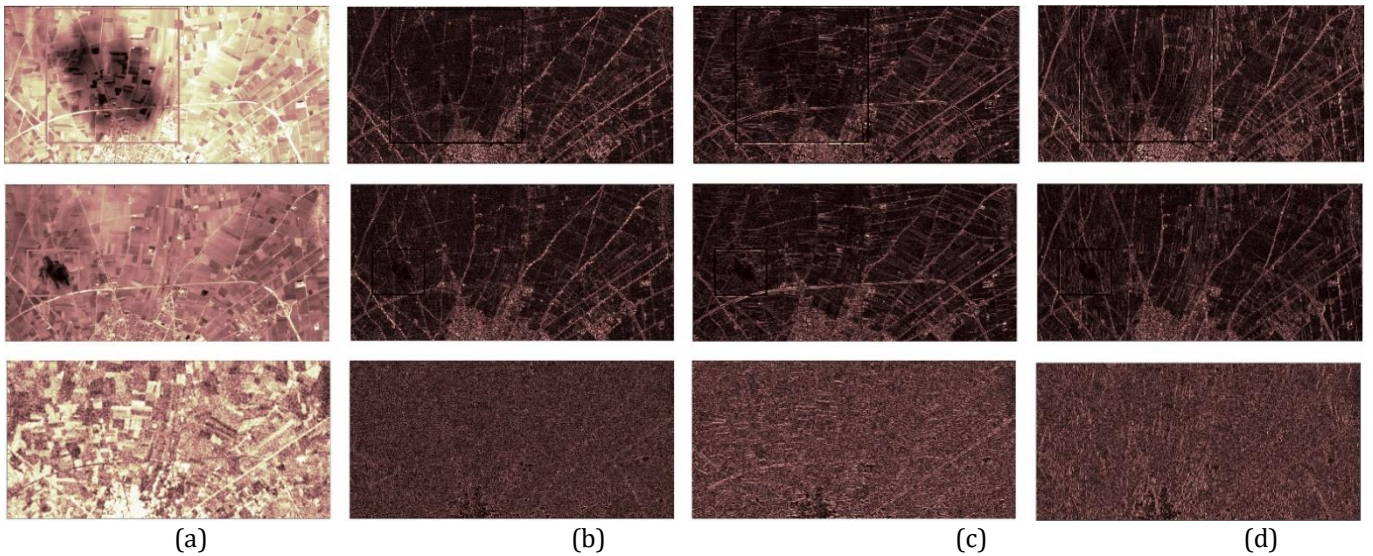
Figure 5. Representation of wavelet coeficients of OP1, OP2 and SAR1 images for "db1" of level 1 (a) approximation (b) diagonal (c) horizontal (d) vertical

Table 3. Fusion rules used in combining the wavelet coefficients.

Approximation Coefficient.	Detail Coefficient
Max	Max
Max	Min
Max	Mean
Min	Min
Min	Max
Min	Mean
Mean	Mean
Mean	Max
Mean	Min

3.1. OP1-OP2 Image Fusion

In this section, fusion of optical images were evaluated. 1710 fused images were obtained using OP1 and OP2 images. Results are sorted by SSI values. The fusion parameters and metric values for the top 10 highest SSI values between the OP1 and the fused images are given in Table 4. The results for the 10 highest SSI values between OP2 and fused images are given in Table 5. The Fus1 and Fus11 fused images with the best SSI value in the Table 4-5 are given in Fig. 6 and Fig .7. SSI values of the Fus1 image with OP1 and OP2 images were respectively 0,86 and 0,56. Thus, the Fus1 image is more similar to the OP1 image. On other hand, SSI values of the Fus11 image and original images were calculated as 0,54 and 0,84. Unlike Fus1, the Fus11 is more similar to the OP2 image. However, the Fus1 is better than the Fus 11 in terms of clarity.

Figure 6. The Fused image of OP1-OP2 according to the Fus1 parameters in Table 4

Figure 7. The Fused image of OP1-OP2 according to the Fus11 parameters in Table 5

Table 4. Fusion parameters and quality metrics of fusion of OP1 and OP2 images (selected by SSI of OP1)

Fused Image Label	Fusion Parameters				Quality Metrics								
	Level	Wavelet packet	Fusion Rule			OP2					OP1			
			Approx. Coef.	Detail Coef.	H	MSE	PSNR	SSI	FSI	MSE	PSNR	SSI	FSIM
Fus1	1	fk8	max	mean	7,69	6673,79	9,89	0,56	0,81	533,69	20,86	0,86	0,96
Fus2	8	rbio1.3	max	max	7,77	6754,43	9,83	0,48	0,81	264,03	23,91	0,86	0,94
Fus3	1	coif3	max	mean	7,68	6667,14	9,89	0,56	0,81	539,23	20,81	0,86	0,96
Fus4	1	fk6	max	mean	7,69	6668,70	9,89	0,56	0,81	534,70	20,85	0,86	0,96
Fus5	1	coif2	max	mean	7,68	6663,90	9,89	0,56	0,81	540,25	20,80	0,86	0,96
Fus6	1	dmey	max	mean	7,69	6672,21	9,89	0,56	0,81	536,99	20,83	0,86	0,96
Fus7	1	db3	max	mean	7,69	6667,97	9,89	0,56	0,81	534,60	20,85	0,86	0,96
Fus8	1	sym3	max	mean	7,69	6667,97	9,89	0,56	0,81	534,60	20,85	0,86	0,96
Fus9	1	fk8	max	max	7,69	6718,42	9,86	0,55	0,81	538,87	20,82	0,86	0,96
Fus10	1	rbio1.5	max	mean	7,69	6660,34	9,90	0,56	0,81	536,53	20,83	0,86	0,96

Table 5. Fusion parameters and quality metrics for fusion of OP1 and OP2 images (selected by SSI of OP2)

Fused Image Label	Fusion Parameters				Quality Metrics								
	Level	Wavelet packet	Fusion Rule			OP2					OP1			
			Approx. Coef.	Detail Coef.	H	MSE	PSNR	SSI	FSIM	MSE	PSNR	SSI	FSIM
Fus11	1	fk8	min	min	7,05	545,40	20,76	0,84	0,94	6755,03	9,83	0,54	0,81
Fus12	1	db3	min	min	7,04	546,46	20,76	0,84	0,94	6754,36	9,83	0,54	0,81
Fus13	1	sym3	min	min	7,04	546,46	20,76	0,84	0,94	6754,36	9,83	0,54	0,81
Fus14	1	fk8	min	mean	7,06	534,23	20,85	0,84	0,94	6688,65	9,88	0,57	0,81
Fus15	1	dmey	min	min	7,05	546,30	20,76	0,84	0,94	6753,48	9,84	0,54	0,81
Fus16	1	fk6	min	min	7,04	547,15	20,75	0,84	0,94	6753,36	9,84	0,54	0,81
Fus17	1	coif3	min	min	7,05	550,03	20,73	0,84	0,94	6749,97	9,84	0,54	0,81
Fus18	1	fk6	min	mean	7,06	535,25	20,85	0,84	0,94	6684,41	9,88	0,57	0,81
Fus19	1	db3	min	mean	7,06	535,14	20,85	0,84	0,94	6682,48	9,88	0,57	0,82
Fus20	1	sym3	min	mean	7,06	535,14	20,85	0,84	0,94	6682,48	9,88	0,57	0,82

3.2. OP1-SAR1 Image Fusion

In this section, the performance of the fusion of OP1 and SAR1 images are investigated. The fusion parameters and metric values with the highest similarity between the fused and SAR1 images are given in Table 6 for top ten results. Besides, the fusion parameters and metric values with the highest similarity between the fused and OP1 images are given in Table 7 for top ten results. Whereas the highest SSI value between SAR1 and fused images is 0,78, the highest SSI value between OP2 and fused images is 0,46. The fused images (Fus21 and Fus31) are shown in Fig. 8 and Fig. 9. As seen from the fused images, the missing regions in optical images were improved by SAR images.

Table 6. Fusion parameters and quality metrics for fusion of OP1 and SAR1 images (selected by SSI of SAR1)

| Fused Image Label | Fusion Parameters | | | | Quality Metrics | | | | | | | | |
| | Level | Wavelet packet | Fusion Rule | | OP1 | | | | | SAR1 | | | |
			Approx. Coef.	Detail Coef.	H	MSE	PSNR	SSI	FSI	MSE	PSNR	SSI	FSI
Fus21	5	rbio1.3	mean	max	7,74	4234,11	11,86	0,23	0,66	2090,60	14,93	0,78	0,88
Fus22	4	rbio1.3	mean	max	7,74	3701,92	12,45	0,24	0,67	2156,31	14,79	0,78	0,86
Fus23	5	coif2	mean	max	7,75	4230,84	11,87	0,22	0,66	2109,38	14,89	0,78	0,88
Fus24	5	db3	mean	max	7,74	4254,31	11,84	0,22	0,66	2111,84	14,88	0,78	0,87
Fus25	5	sym3	mean	max	7,74	4254,31	11,84	0,22	0,66	2111,84	14,88	0,78	0,87
Fus26	5	coif1	mean	max	7,75	4285,21	11,81	0,22	0,66	2102,16	14,90	0,78	0,87
Fus27	5	fk6	mean	max	7,75	4263,14	11,83	0,22	0,66	2105,35	14,90	0,78	0,87
Fus28	4	coif2	mean	max	7,74	3715,68	12,43	0,23	0,67	2178,87	14,75	0,78	0,86
Fus29	4	rbio1.5	mean	max	7,73	3693,07	12,46	0,24	0,67	2178,97	14,75	0,77	0,86
Fus30	5	rbio1.5	mean	max	7,74	4252,96	11,84	0,22	0,66	2120,25	14,87	0,77	0,88

Table 7. Fusion parameters and quality metrics for fusion of OP1 and SAR1 images (selected by SSI of OP1)

| Fused Image Label | Fusion Parameters | | | | Quality Metrics | | | | | | | | |
| | Level | Wavelet packet | Fusion Rule | | OP1 | | | | | SAR1 | | | |
			Approx. Coef.	Detail Coef.	H	MSE	PSNR	SSI	FSI	MSE	PSNR	SSI	FSI
Fus31	1	dmey	max	max	7,48	4290,36	11,81	0,46	0,76	4362,61	11,73	0,54	0,77
Fus32	1	rbio1.5	max	mean	7,51	4288,86	11,81	0,45	0,77	4256,68	11,84	0,55	0,78
Fus33	1	rbio1.5	max	max	7,49	4273,07	11,82	0,45	0,77	4309,69	11,79	0,55	0,78
Fus34	1	coif3	max	max	7,48	4299,69	11,80	0,45	0,76	4350,66	11,75	0,55	0,78
Fus35	1	rbio1.3	max	mean	7,51	4279,61	11,82	0,45	0,77	4241,61	11,86	0,56	0,78
Fus36	1	dmey	max	mean	7,49	4326,09	11,77	0,45	0,76	4298,56	11,80	0,55	0,78
Fus37	1	coif3	max	mean	7,49	4323,20	11,77	0,44	0,76	4291,77	11,80	0,55	0,78
Fus38	1	fk8	max	mean	7,49	4318,33	11,78	0,44	0,76	4290,36	11,81	0,55	0,78
Fus39	1	coif2	max	mean	7,49	4319,51	11,78	0,44	0,76	4285,66	11,81	0,55	0,78
Fus40	1	fk8	max	max	7,48	4298,62	11,80	0,44	0,76	4346,17	11,75	0,55	0,78
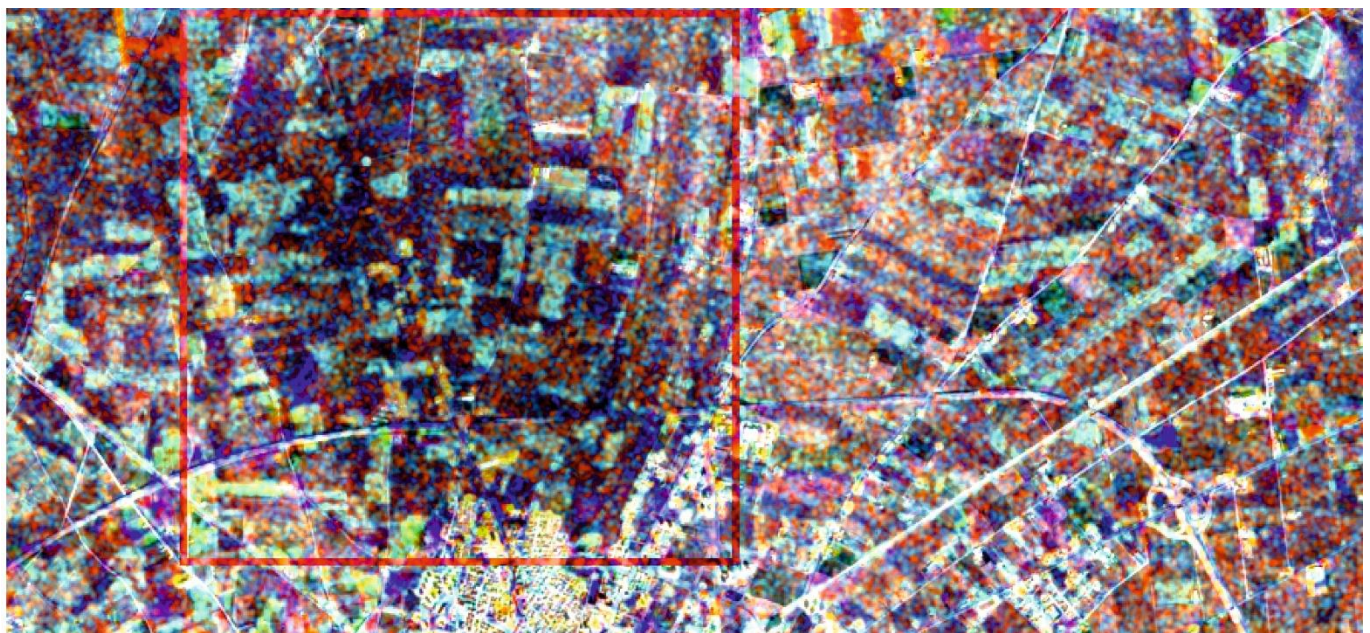
Figure 8. The Fused Image of OP1-SAR1 according to the Fus21 parameters in Table 6

Figure 9. The Fused Image of OP1-SAR1 according to the Fus31 parameters in Table 7

3.3. OP2-SAR1 Image Fusion

In this section, the OP2 and SAR1 images were fused. The best results for ten fused images are given in Table 8 and Table 9. The highest SSI between fused and SAR1 images was obtained with " rbio1.3" wavelet packet as 0,91. The Fus41 image is indicated in Fig. 10. On the other hand, Fus51 image with highest SSI was obtained with "dmey" wavelet packet. SSI between Fus51 and OP2 images is 0,72 and Fus51 is shown in Fig. 11. As can be seen from Fig. 9, the missing regions in the optical images were improved by SAR image. However, the Fus51 includes still missing regions in Fig. 11.

Figure 10. The Fused Image of OP2-SAR1 according to the Fus41 parameters in Table 8

Figure 11. The Fused Image of OP2-SAR1 according to the Fus51 parameters in Table 8

Table 8. Fusion parameters and quality metrics for fusion of OP2 and SAR1 images (selected by SSI of SAR1)

Fused Image Label	Level	Wavelet packet	Fusion Rule		OP2					SAR1			
			Approx. Coef.	Detail Coef.	H	MSE	PSNR	SSI	FSI	MSE	PSNR	SSI	FSI
Fus41	4	rbio1.3	max	max	7,80	7827,62	9,19	0,12	0,60	507,34	21,08	0,91	0,93
Fus42	3	rbio1.3	max	max	7,77	7877,23	9,17	0,12	0,60	500,55	21,14	0,91	0,93
Fus43	4	rbio1.5	max	max	7,80	7853,11	9,18	0,12	0,60	506,93	21,08	0,91	0,93
Fus44	3	rbio1.5	max	max	7,77	7896,71	9,16	0,12	0,60	501,51	21,13	0,91	0,93
Fus45	4	db2	max	max	7,80	7888,54	9,16	0,12	0,60	516,04	21,00	0,91	0,93
Fus46	4	sym2	max	max	7,80	7888,54	9,16	0,12	0,60	516,04	21,00	0,91	0,93
Fus47	5	coif1	max	max	7,81	7821,10	9,20	0,11	0,60	539,89	20,81	0,91	0,93
Fus48	3	db2	max	max	7,77	7933,52	9,14	0,12	0,60	519,02	20,98	0,91	0,93
Fus49	3	sym2	max	max	7,77	7933,52	9,14	0,12	0,60	519,02	20,98	0,91	0,93
Fus50	4	rbio1.3	max	max	7,80	7827,62	9,19	0,12	0,60	507,34	21,08	0,91	0,93

Table 9. Fusion parameters and quality metrics for fusion of OP2 and SAR1 images (selected by SSI of OP2)

Fused Image Label	Level	Wavelet packet	Fusion Rule		OP2					SAR1			
			Approx. Coef.	Detail Coef.	H	MSE	PSNR	SSI	FSI	MSE	PSNR	SSI	FSI
Fus51	1	dmey	min	mean	6,92	580,25	20,49	0,72	0,85	7992,97	9,10	0,26	0,66
Fus52	1	rbio1.5	min	mean	6,93	565,55	20,61	0,72	0,85	7937,16	9,13	0,27	0,66
Fus53	1	rbio1.3	min	min	6,91	589,98	20,42	0,72	0,85	7975,33	9,11	0,24	0,66
Fus54	1	coif3	min	mean	6,92	581,79	20,48	0,72	0,85	7979,99	9,11	0,26	0,66
Fus55	1	rbio1.5	min	min	6,91	592,74	20,40	0,72	0,85	7975,44	9,11	0,25	0,66
Fus56	2	rbio1.3	min	min	6,88	563,32	20,62	0,71	0,85	7971,97	9,12	0,19	0,64
Fus57	3	rbio1.3	min	min	6,85	541,42	20,80	0,71	0,83	7989,92	9,11	0,12	0,60
Fus58	1	fk8	min	mean	6,92	583,83	20,47	0,71	0,85	7974,93	9,11	0,27	0,66
Fus59	1	rbio1.3	min	mean	6,93	567,64	20,59	0,71	0,85	7910,54	9,15	0,27	0,66
Fus60	1	db1	min	min	6,90	600,63	20,34	0,71	0,85	8002,30	9,10	0,23	0,66

4. CONCLUSION

In this study, wavelet-based fusion of optical-optical and optical-SAR images were investigated. Optical and SAR images were obtained from Sentinel-1 and Sentinel-2 satellites datasets. The four main wavelet coefficients of original images were obtained. The optical images were fused with optical and SAR images. Images were analysed for 19 different wavelet packets with up to 10

decomposition levels. The wavelet coefficients are combined by applying the fusion rule that includes the maximum, minimum and mean methods. Under these parameters' conditions, a total of 1710 fused images were obtained for each fusion application. Fused images were evaluated using 5 different metric criteria. In each fusion application, 20 fused images most similar to the original images were selected by SSI values. It was observed that the missing regions in the optical images

were improved in fused images. However, it was determined that the most effective wavelet-packets changes according to the change in the images to be fused. The most effective wavelet packets in 3 different fusions were found as "dmey", "fk8" and "rbio1.3". The results obtained in this article reveal that there are many parameters in the fusion process and thousands of combinations must be evaluated to obtain the most informative and clear image. However, in future studies, instead of evaluating all possible fused images, optimal fusion parameters can be obtained with natural inspired optimization algorithms.

Author contributions

Huseyin Duysak: Investigation, Data preparation and Image fusion, **Enes Yigit**: Evaluation of the images, Writing-Reviewing and Editing.

Conflicts of interest

The authors declare no conflicts of interest.

REFERENCES

Aslan M F, Durdu A & Sabanci K (2019). Fusion of CT and MR Liver Images by SURF-Based Registration. *International Journal of Intelligent Systems and Applications in Engineering*, *7*(4), SE-Research Article). doi:10.18201/ijisae.2019457233

Foumelis M, Blasco J M D, Desnos Y, Engdahl M, Fernandez D, Veci L, … Wong C (2018). *Esa Snap - Stamps Integrated Processing for Sentinel-1 Persistent Scatterer Interferometry*. In *IGARSS 2018 - 2018 IEEE International Geoscience and Remote Sensing Symposium*, 1364–1367. doi:10.1109/IGARSS.2018.8519545

Ghorbanzadeh O, Didehban K, Rasouli H, Kamran K V, Feizizadeh, B., & Blaschke, T. (2020). An application of sentinel-1, sentinel-2, and GNSS data for landslide susceptibility mapping. *ISPRS International Journal of Geo-Information*, *9*(10), 561.

Hemdan E E-D (2021). An efficient and robust watermarking approach based on single value decompression, multi-level DWT, and wavelet fusion with scrambled medical images. *Multimedia Tools and Applications*, *80*(2), 1749–1777. doi:10.1007/s11042-020-09769-7

James A P & Dasarathy B V (2014). Medical image fusion: A survey of the state of the art. *Information Fusion*, *19*, 4–19. doi:https://doi.org/10.1016/j.inffus.2013.12.002

Khaleghi B, Khamis A, Karray F O & Razavi S N (2013). Multisensor data fusion: A review of the state-of-the-art. *Information Fusion*, *14*(1), 28–44. doi:https://doi.org/10.1016/j.inffus.2011.08.001

Kulkarni S C & Rege P P (2020). Pixel level fusion techniques for SAR and optical images: A review. *Information Fusion*, *59*, 13–29. doi:https://doi.org/10.1016/j.inffus.2020.01.003

Pajares G & Manuel de la Cruz J (2004). A wavelet-based image fusion tutorial. *Pattern Recognition*, *37*(9), 1855–1872. doi:https://doi.org/10.1016/j.patcog.2004.03.010

Rajah P, Odindi J & Mutanga O (2018). Feature level image fusion of optical imagery and Synthetic Aperture Radar (SAR) for invasive alien plant species detection and mapping. *Remote Sensing Applications: Society and Environment*, *10*, 198–208. doi:https://doi.org/10.1016/j.rsase.2018.04.007

Shah E, Jayaprasad P & James M E (2019). Image fusion of SAR and optical images for identifying antarctic ice features. *Journal of the Indian Society of Remote Sensing*, *47*(12), 2113–2127.

Veloso A, Mermoz S, Bouvet A, Le Toan T, Planells M, Dejoux J-F & Ceschia E (2017). Understanding the temporal behavior of crops using Sentinel-1 and Sentinel-2-like data for agricultural applications. *Remote Sensing of Environment*, *199*, 415–426. doi:https://doi.org/10.1016/j.rse.2017.07.015

Yommy A S, Liu R & Wu A S (2015). *SAR Image Despeckling Using Refined Lee Filter*. In *2015 7th International Conference on Intelligent Human-Machine Systems and Cybernetics*, 2, 260–265. doi:10.1109/IHMSC.2015.236